



## Evaluation of The Efficacy of Bioactive Glass /G-C<sub>3</sub>N<sub>4</sub> Hybrid Nanocomposites Embedded In B72 Matrix For Consolidating Archaeological Stuccoes



Mohammed S. A. Khedr <sup>1,†</sup>, Mona F. Ali <sup>2</sup>, Ahmed N. Emam <sup>3</sup>, Abdullah M. A. Kamel <sup>2</sup>,  
Manal A. A. EL Ghanam <sup>4</sup>

<sup>1</sup> Head of the First Aid Lab, National Museum of Egyptian Civilization, Ministry of Antiquities

<sup>2</sup> Conservation Department, Faculty of Archaeology, Cairo University, 12613 Giza, Egypt

<sup>3</sup> Refractories, Ceramics and Building Materials Department, Advanced Material Technology & Mineral Resources Research Institute, Nanomedicine & Tissue Engineering Research Lab, Medical Research Centre of Excellence, National Research Centre (NRC), El Bohouth St., Dokki, 12622 Cairo, Egypt.

<sup>4</sup> A Head of the central administration for maintenance and restoration, Ministry of Antiquities, Cairo, Egypt.

### Abstract

Stucco monuments are highly susceptible to damage, and their consolidation requires the evaluation of new and advanced materials. Nanocomposites have shown highly promising consolidating results when applied to many historic materials, like stone and mural paintings. The current experimental study evaluates the effectiveness of bioactive glass nanoparticles (BG NPs) added to graphite carbon nitride (g-C<sub>3</sub>N<sub>4</sub>) and mixed with paraloid (B-72) in acetone. Herein, bioactive glass nanoparticles and graphitic carbon nitride nanosheets have been prepared through sol-gel and thermal decomposition chemical routes, respectively. The physicochemical properties of the as-prepared nanopowders have been investigated using transmission electron microscopy (TEM), X-ray diffraction (XRD), and Fourier transform infrared (FT-IR). In addition, the colloidal properties were investigated using the dynamic light scattering technique. The evaluation protocol outlined a six-step process to assess the suitability of standard samples consolidated with nanocomposites after undergoing artificial aging procedures. The study involves monitoring the changes in consolidated samples after exposure to various conditions by using a digital microscope and SEM to identify the appearance of the consolidated stucco samples after applying the selected nanocomposites and after their artificial aging procedures. Color change is measured using a colorimeter, and comparisons are made between samples before and after aging. Physical and mechanical properties are determined, and the contact angle is measured to determine the hydrophobicity or hydrophilicity. The obtained results indicate that bioactive glass/g-C<sub>3</sub>N<sub>4</sub> hybrid nanocomposites with a composition of BG 0.5%, g-C<sub>3</sub>N<sub>4</sub> 1%, and B-72 3% achieved the best consolidating results among the proposed mixtures for stucco samples.

**Keywords:** Stucco, Hybrid, Investigation, Color change, Contact angle, SEM, XRD.

### 1. Introduction

Inorganic artifacts such as stucco, stone, and plaster are constantly under threat from degradation issues, such as biological or chemical deterioration, which can significantly impact their structural integrity and mechanical strength [1, 2]. Common stucco deterioration aspects, including changes in composition disintegration, reduced cohesion of surface layers, spalling from the substrate, buckling deformation, crack occurrence, and color changes [3], further underline the urgency of our role in heritage conservation. A proper rehabilitation approach to protecting the value of heritage buildings and their surface covering is, therefore, not just a choice but a necessity. Experimental studies help assess the effectiveness of materials and methods for safeguarding stucco artifacts [4, 5]. Stucco conservation involves incorporating worn and degraded binder into the treated material's structure or joining split sections to the substrate and filling in missing areas. Structural consolidation is carried out with carefully chosen consolidating agents, stabilizing the damaged Stucco system, or replacing the "leached" original binder material with a substance with equal qualities [6]. Hybrid nanocomposites, with their unique physical properties, features, and changes, have been found to be effective in consolidating stucco artifacts in museums [7]. Nanomaterials (1–100 nm) have a higher specific surface area than larger-scale materials, and they penetrate deeply into the damaged surfaces, offering a promising solution to the challenges we face [8, 9]. The acquisition of new systems, such as metal oxides and hydroxides (i.e., TiO<sub>2</sub>, ZnO, Ca(OH)<sub>2</sub>, Mg(OH)<sub>2</sub>), and metal nanoparticles (i.e., Au, Ag, and Pt), and their ability to effectively consolidate on diverse artifacts and works of art have been documented in the literature [10, 11]. Metal oxide nanoparticles have been employed to protect building surfaces from biofilm formation for the past decade. The potential of these nanoparticles in the conservation and restoration of cultural property has been demonstrated for the consolidation of dissolving materials, self-cleaning, material surface improvement, and as a biocide to decrease biodegradation [12]. Nanotechnology, a field that has

\*Corresponding author e-mail: [mohamed.soliman@nmecc.gov.eg](mailto:mohamed.soliman@nmecc.gov.eg);

(Mohammed S. A. Khedr). Receive Date: 07 May 2024, Revise Date: 16 June 2024, Accept Date: 23 June 2024

DOI: 10.21608/ejchem.2024.287769.9685

©2025 National Information and Documentation Center (NIDOC)

been used for thousands of years unintentionally, with vital systems in the human body manufacturing small devices and cells that reach the nanoscale, holds the promise of a brighter future for cultural heritage preservation. Glassmakers in the Middle Ages and Arabs were among the first to use this technique, using colloidal gold granules in stained glass windows and Damascene swords [13, 14]. Bioactive glass is an amorphous material that has a disordered arrangement of atoms due to the rapid cooling of the molten ceramic. For bone tissue engineering, bioactive glasses can be silica-based, phosphate-based, or borate-based amorphous materials [15–17]. Among the various types of bioactive glasses, the most common and readily used in clinical applications is Bioglass 45S5 (46.1% SiO<sub>2</sub>, 24.4% NaO, 26.9% CaO, and 2.6% P<sub>2</sub>O<sub>5</sub>; mol%). The term 45S5 signifies that the composition consists of 45% weight of SiO<sub>2</sub>, S for silica as the network former, and a 5 to 1 molar ratio of Ca to P (in the form of CaO and P<sub>2</sub>O<sub>5</sub>) [18, 19]. In addition, bioactive glasses belong to a particular class of biomaterials that can induce the precipitation of a layer of hydroxyapatite or hydroxycarbonate apatite, a main constituent of bone tissue, when put in contact with body fluid, leading to the formation of a chemical bond with living tissue [20–22]. Hydroxyapatite layers have benefits when used as consolidating materials [23, 24]. From this standpoint, the idea of using bioactive glasses (BGs) to consolidate stucco monuments came about because it is known that the stucco mixture consists of gypsum and calcite, the basis of which is calcium. Graphite carbon nitride (g-C<sub>3</sub>N<sub>4</sub>) nanomaterials are synthetic polymers with electron-rich properties, basic surface functionalities, and H-bonding patterns, making them a potential replacement for carbon in material applications [25]. They are attractive nonmetallic photocatalysts due to their sensitivity to visible light, resistance to photocorrosion and oxidation, chemical stability, low toxicity to humans, and the ability to change optical properties [26, 27]. Despite their advantages, g-C<sub>3</sub>N<sub>4</sub> exhibits low photocatalytic activity due to low visible light absorption, a low specific surface area, and a fast charge recombination rate. Despite these challenges, there are conflicting explanations on how the structure and composition of g-C<sub>3</sub>N<sub>4</sub> affect its antibacterial efficacy, limiting the priority of designing g-C<sub>3</sub>N<sub>4</sub> materials for specific performance goals [28].

The choice of the right materials for consolidation and adhesion purposes is a critical aspect of our work in the field of cultural heritage preservation. Paraloid, a popular polymeric material used for archaeological materials [29], has a low degree of penetration, which is a significant disadvantage in consolidation processes [30]. The physical and mechanical properties of acrylic polymers, especially the various types of paraloid, play a major role in the use of these polymers in the archaeological field [31]. Paraloid B-72 Solid Grade Thermoplastic Acrylic Resin is a lower T<sub>g</sub> (40 °C) acrylic resin capable of forming softer films. It is characterized by low reactivity with sensitive materials.

Polymeric hybrid nanocomposites are materials with unique properties thanks to the interaction between the added particles and the polymer. Natural and synthetic polymers, biopolymers, and plastics have nanoparticles embedded in them. The right selection of consolidate involves selecting the proper polymer, nanoparticles, and preparation technique. Common methods include in-situ polymerization, the Sol-Gel method, and solution dispersion [32, 33]. PMNCS, a crucial nanocomposite, is characterized by self-cleaning, water resistance, microbiology resistance, and ultraviolet ray resistance, making it a promising option for cultural heritage preservation. However, nanocomposites can agglomerate due to grafting or adding materials. Modern techniques, such as good dispersion of nanomaterials, direct mixing of polymers and nanomaterials, instantaneous emulsion polymerization, and ultrasonic methods, help avoid defects in nanocomposites [34–37].

To the best of our knowledge, no studies have been conducted to evaluate the effectiveness of hybrid nanocomposites consisting of bioactive glass nanoparticles (BG NPs) combined with graphite carbon nitride (g-C<sub>3</sub>N<sub>4</sub>) and paraloid (B-72) in acetone. In this study, bioactive glass nanoparticles and graphitic carbon nitride nanosheets were prepared using sol-gel and thermal decomposition chemical methods. The physical and chemical properties of the resulting nanopowders were analyzed using techniques such as transmission electron microscopy (TEM), x-ray diffraction (XRD), and Fourier transform infrared (FT-IR). Furthermore, dynamic light scattering was used to investigate the colloidal properties. A six-step protocol was developed to evaluate the suitability of standard samples consolidated with nanocomposites after undergoing aging processes. The evaluation process involves analyzing changes in the consolidated samples after exposure to various environmental conditions using digital microscopes and scanning electron microscopy (SEM). The appearance of the samples was assessed after the nanocomposites were added and after the artificial aging process. Color changes were measured and compared using samples before and after artificial aging. Finally, the physical and mechanical properties, as well as the contact angle, were measured to assess the hydrophobicity rate. So, the main aim of this article showing the importance of the consolidation's effectiveness of stucco objects.

## 2. Materials and methods

### 2.1. Materials

Urea (CO(NH<sub>2</sub>)<sub>2</sub>, 95%), Tetraethyl orthosilicate (TEOS, Si(OC<sub>2</sub>H<sub>5</sub>)<sub>4</sub>, 99.99%), Triethyl phosphate (TEP, (C<sub>2</sub>H<sub>5</sub>)<sub>3</sub>PO<sub>4</sub>, 98%, LOBA Chemie, India), Ammonia (NH<sub>4</sub>OH, 28%), and Calcium nitrate tetrahydrate (Ca(NO<sub>3</sub>)<sub>2</sub>·4H<sub>2</sub>O, 99%).

### 2.2. Methodology

#### 2.2.1. Preparation of bioactive glass 45S5 (BG) nanostructures

Bioactive glass nanoparticles (BG) based on this were synthesized by a modified sol-gel method [38–40]. In brief, TEOS was added dropwise to a mixture of distilled water, ethanol, and nitric acid, followed by stirring for 1 hour to achieve the complete acid hydrolysis of TEOS. Thereafter, TEP and Ca(NO<sub>3</sub>)<sub>2</sub>·4H<sub>2</sub>O were added while stirring was continued for 1 h after each addition, and then the whole solution was placed in a conventional ultrasonic bath. Meanwhile, ammonia solution was added dropwise to the mixture while continuous agitation by mechanical stirring was carried out to prevent the formation of a bulk gel. The solution was completely transformed into a white gel in a few minutes. Finally, the prepared gel was dried at 75°C for 2 days in a drying oven, and then it was subjected to heat treatment at 700°C for 3 hours at a rate of 3°C/min to stabilize and convert the gel to glass [41].

### 2.2.2. Preparation of graphitic carbon nitride (g-C<sub>3</sub>N<sub>4</sub>) nano-sheets

Graphitic carbon nitride (g-C<sub>3</sub>N<sub>4</sub>) was synthesized using a thermally induced copolymerization technique with urea as the precursor, as previously reported [42, 43]. In a typical run, 100 g of urea was placed in a crucible with a loose lid and heated to 550 °C at a rate of 10 °C/min. The crucible was left at 550 °C for 4 hours in a muffle furnace. When the temperature was reduced to room temperature, solid, pristine g-C<sub>3</sub>N<sub>4</sub> was produced and ground to a powder for subsequent usage.

### 2.2.3. Preparation of BG/g-C<sub>3</sub>N<sub>4</sub> – B72 hybrid nanocomposites

BG/g-C<sub>3</sub>N<sub>4</sub> hybrid nanocomposites embedded in B72 polymeric matrix have been fabricated via physical mixing under vigorous high-energy ultra-sonication, as follows: the ratio of BG/g-C<sub>3</sub>N<sub>4</sub> was adjusted as reported in Table 1. The as-prepared nanopowders were added to an acetone solution of 3 wt/v% of B72 polymeric matrix. The mixture was subjected to high-energy ultrasonication with an amplitude of 50% for 30 min with a pulse interval of 10 s.

Table 1: Composition of as-prepared BG/g-C<sub>3</sub>N<sub>4</sub> hybrid nanocomposites

Samples	Hybrid Nanocomposites Composition
A	BG NPs 0.5 wt/wt% + g-C <sub>3</sub> N <sub>4</sub> 1 wt/wt% + B72 3 wt/v%
A+	BG NPs 1.0 wt/wt% + g-C <sub>3</sub> N <sub>4</sub> 1 wt/wt% + B 72 3 wt/v%
A <sup>++</sup>	BG NPs 3.0 wt/wt% + g-C <sub>3</sub> N <sub>4</sub> 1 wt/wt% + B 72 3 wt/v%
F	BG NPs 0.5 wt/wt% + g-C <sub>3</sub> N <sub>4</sub> 2 wt/wt% + B 72 3 wt/v%
F <sup>+</sup>	BG NPs 1.0 wt/wt% + g-C <sub>3</sub> N <sub>4</sub> 2 wt/wt% + B 72 3 wt/v%
F <sup>++</sup>	BG NPs 3.0 wt/wt% + g-C <sub>3</sub> N <sub>4</sub> 2 wt/wt% + B 72 3 wt/v%

## 2.3 Procedures of sample preparation and accelerated artificial ageing

### 2.3.1 Sample Preparation

The experimental samples after conducting tests and analysis on the stucco mask have been investigated according to previous reports (a stucco mask from the National Museum of Ancient Egyptian Civilization, NMEC) [44]. In such a case, the experimental samples were prepared so that they were like the components of the stucco artifact. The mixture ingredients were composed of hemihydrate (68.2 parts), hydrated lime (7.2 parts), quartz (sand grains) (3 parts), and dolomite (5.25 parts). Experiment samples were made with the following dimensions (3 x 3 x 3 cm<sup>3</sup>, ASTM C97/C97M, 2015), which were categorized into two groups (A) and (F), with 9 samples in each group, as shown in Table 2.3.

The test samples were put through several man-made weathering cycles, as shown in Fig. 1 (Humidity, Drying, and Weathering Cycles with Sodium Chloride Salt). The experimental samples were evaluated after performing the different artificial weathering cycles. To assess the suitability of the samples, the evaluation involved creating a six-step protocol in which the level of loss that happens on samples after being exposed to different conditions, like a USB digital microscope, an SEM, measuring color change, figuring out physical and mechanical properties, and contact angle, is used to set standard standards before and after they are exposed to accelerated artificial aging processes.



Fig. 1: shows the experimental samples in industrial weathering cycles, where points (A) show the experimental samples before artificial aging, points (B-C) show the experimental samples during different industrial weathering cycles, and point (D) show the experimental samples after industrial Artificial aging.

Some mechanical cleaning work (scalpers, scalpels, brushes of all kinds, and distilled water) was carried out on the experimental samples to remove and extract some of the salt calcifications that formed during the industrial Artificial aging cycles, as shown in Fig. 2, so that the experimental samples could be ready for the next stages of the process. Consolidation with the as-prepared hybrid nanocomposites as previously mentioned in Table 1, thus the effect under study may have been completely simulated. After that, the general appearance examination was carried out, and the samples were cleaned with a piece of cloth and examined with the naked eye to ensure that the surface was clean, smooth, and level, free of bumps, cracks, dimpling, numbness, peeling and separation.

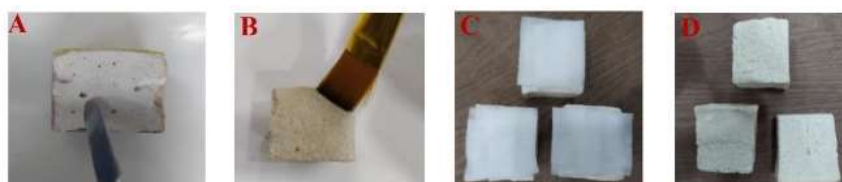


Fig. 2 shows the experimental samples in the mechanical cleaning stages. Point (A) shows the use of scalpels to remove salt calcifications; Point (B) shows the use of brushes; Point (C) compresses to extract salts; and Point (D) shows the samples after the mechanical cleaning stages.

### 2.3.2 Accelerated artificial ageing

Upon the application of the BG/g-C3N4 hybrid nanocomposites with their different concentrations to the experimental samples, various artificial weathering cycles were carried out [45], as follows:

- Humidity-Drying Cycles. The samples were dried before the start of the test at 105 °C until the weight was stable, then the samples were weighed, as illustrated in Tables 2 and 3, respectively. Then the treated samples were immersed in water for four hours, then dried in a closed oven at a temperature of 60° ( $\pm 15^\circ$ ) for 18 hours. This is followed by leaving the samples in the room atmosphere for 4 hours in order to stabilize them. These steps are repeated for 10 cycles, and the weights are followed up after each cycle, and the weights are recorded accurately.
- Cycles of weathering with sodium chloride salt. On the same samples, salt cycles were performed, followed by drying before the start of the test at 105 °C until the weight was stable, then the samples were weighed as illustrated in Tables 2 and 3. Then the samples were immersed in a 10% solution of sodium chloride salt in water for 3 hours. The samples were then dried in a closed oven at a temperature of  $60 \pm 15^\circ\text{C}$  for  $16 \pm 2$  h. The samples were then placed in a room atmosphere for 3 hours, and these steps were repeated for 10 cycles.

Finally, the operation of artificial weathering cycles was evaluated, where the average weight and surface changes of the samples were monitored, and comparisons were made for the samples before and after the different stages as well as before and after artificial aging (Group A, Table 2) and (Group F, Table 3).

Table 2: shows the weight of the experimental samples (Group A) between the different stages and tests.

Samples Stucco before Artificial aging	Weight before drying (g)	Weight after drying(g) 105 $\pm$ 2°C	Sample weight After Artificial aging tests before the nanocomposite	Weight after nanocomposite application	Samples after the humidity drying cycles	Samples after the weathering cycles with sodium chloride salt
1A	31.63	29.45	30.22	32.92	32.91	31.98
2A	29.98	27.90	28.81	31.51	31.40	30.65
3A	32.92	29.28	30.12	33.01	33.13	32.60
<b>Average</b>	<b>31.51</b>	<b>28.87</b>	<b>29.71</b>	<b>32.48</b>	<b>31.83</b>	<b>31.74</b>
1A <sup>+</sup>	30.70	27.75	28.66	30.30	30.29	30.01
2A <sup>+</sup>	31.56	29.48	30.15	33.01	32.89	31.19
3A <sup>+</sup>	30.48	27.53	28.14	31.13	30.09	29.39
<b>Average</b>	<b>30.91</b>	<b>28.75</b>	<b>28.98</b>	<b>31.48</b>	<b>31.09</b>	<b>30.19</b>
1A <sup>++</sup>	31.42	28.01	28.87	31.69	31.59	31.22
2A <sup>++</sup>	31.59	27.25	28.11	31.30	31.48	31.13
3A <sup>++</sup>	31.94	28.04	28.92	31.08	31.09	30.45
<b>Average</b>	<b>31.65</b>	<b>27.76</b>	<b>28.63</b>	<b>31.35</b>	<b>31.38</b>	<b>30.93</b>

Table 3: shows the weight of the experimental samples (Group F) between the different stages and tests.

Samples Stucco before Artificial aging	Weight before drying (g)	Weight after drying(g) 105 $\pm$ 2°C	Sample weight After Artificial aging tests before the nanocomposite	Weight after nanocomposite application	Samples after the humidity drying cycles	Samples after the weathering cycles with sodium chloride salt
1F	30.88	28.62	29.13	32.76	32.80	31.12
2F	31.83	29.46	30.14	33.41	33.53	32.22
3F	30.23	28.17	28.98	32.25	32.38	31.54
<b>Average</b>	<b>30.98</b>	<b>28.75</b>	<b>29.41</b>	<b>32.80</b>	<b>32.90</b>	<b>31.62</b>
1F <sup>+</sup>	29.25	27.15	28.08	30.52	30.55	30.13
2F <sup>+</sup>	29.53	27.64	28.14	31.55	31.61	31.14
3F <sup>+</sup>	29.50	27.51	27.99	31.31	31.32	30.34
<b>Average</b>	<b>29.51</b>	<b>27.43</b>	<b>28.07</b>	<b>31.12</b>	<b>31.16</b>	<b>30.53</b>
1F <sup>++</sup>	27.02	25.36	26.73	28.63	28.71	28.13
2F <sup>++</sup>	29.75	28.02	28.87	31.76	31.60	31.35
3F <sup>++</sup>	29.65	27.55	28.11	31.38	31.43	31.07
<b>Average</b>	<b>28.80</b>	<b>26.97</b>	<b>27.90</b>	<b>30.59</b>	<b>30.58</b>	<b>30.18</b>

### 2.4. Characterization

The morphology of as-prepared BG and g-C3N4 NPs was characterized using the transmission electron microscope (TEM) JEOL, model JEM 2100F, under an operating voltage of 60 kV. The substance was diluted in water at least ten times before to testing. After that, a drop of the fully dispersed diluted specimen was put onto a 200-grid copper mesh covered with carbon

film, then dried at room temperature. In addition, the crystallographic structure has been investigated using X-ray diffraction patterns obtained through the use of milled samples by using the diffractometer model PW 1480 Netherland, operated at 35 kV, using a Cu and Ka radiation wavelength of 1.54056Å. The reference database used for matching is PDF4. Scanning speed: 0.04/sec., start position  $2\theta = 5^\circ$  to end position  $2\theta = 70^\circ$ . Furthermore, FT-IR of the BG and g-C3N4 NPs were obtained from the JASCO FT-IR-460 PLUS Spectrometer (wave length, number range: 4000 to 400  $\text{cm}^{-1}$  at a resolution of 4  $\text{cm}^{-1}$ , single beam).

### 2.5. USB digital microscopes

Some samples of standard were examined using a portable digital microscope with a magnification ratio starting from 10–5010–50 X with the aim of examining and studying the morphological features of the samples. The digital microscope (model PZ01, made by Shenzhen Super Eyes Co. Ltd., China).

### 2.6. Scanning electron microscopy (SEM)

Some samples of the standard were examined using the SEM the SEM Model Quanta 250 FEG (Field Emission Gun) attached to and EDX Unit with an accelerating an accelerating voltage of voltage of 30 KV, a magnification 14x up to 1000000, and a resolution of 1 n. FEI Company, Netherlands, at the Grand Egyptian Museum. It is a very useful tool for evaluating the efficiency of reinforcement materials, the ability of the material to spread, and the extent of bonding between the material and the treated surface [46], as well as for characterizing the surface of experimental samples before and after treatment with nanocomposites, and also through the use of the dispersed phase of electrons, which examines more deeply than secondary electrons, which helps in evaluating the extent of penetration of reinforcement materials in contrast to routine morphological examination [47]. A uniform magnification (2000) was used to make comparisons between the experimental samples correctly.

### 2.7. Determination of the Physical Properties

The specimens' physical characteristics were determined using dry and wet weights. Before the testing, the specimens were dried at 105 °C and weighed before being immersed in distilled water for 20 hours and weighed again [48]. The devices of the Housing and Building National Research Centre in Cairo were used. The physical properties were calculated as follows:

#### 2.7.1. Bulk density

The following equation was used to calculate bulk density in  $\text{g}/\text{cm}^3$ :

$$D = W/V$$

Where: W denotes the starting weight in g and V denotes the volume in  $\text{cm}^3$ .

Using the following equation, the percentage of water absorption (W.A) was determined.

$$W. A = \frac{W_2 - W_1}{W_1} \times 100 = \%$$

W1 and W2 are, respectively, the dry and wet weights in g.

#### 2.7.2. Bulk porosity

The following equation was used to calculate apparent porosity (A.P) in %:

$$A. P = \frac{W_2 - W_1}{V} \times 100 = \%$$

W1 and W2 are the dry and wet weights in g, respectively, and V is the volume in  $\text{cm}^3$  [49].

### 2.8. Compressive Strength measurement.

After identifying the physical properties of these samples, they are mechanically tested to determine the extent of resistance of these mixtures to stresses and pressure on them so that the different conditions of the applied model are simulated [50]. A pressure resistance device was used, consisting of two parts: an upper part, i.e., the source of pressure, and a lower part on which the sample is placed. Pressure is placed on the sample in the upper part until it shatters, and then the extent of these samples' tolerance to various pressure factors is calculated. The samples were also put through compression tests according to ASTM C170, which is a standard test method for measuring the compressive strength of dimension stone.

### 2.9. Change measurement

A color change test was carried out to evaluate the differences between the experimental samples, as shown in Tables (4-5). After treatment and strengthening with nanocomposites and after studying industrial Artificial aging, group (A, F). according to the equation below:

$$\Delta E = \sqrt{(\Delta l)^2 + (\Delta a)^2 + (\Delta b)^2}$$

The color change was measured using a device (PCE-XXM20 Farbmessgerät) to identify the extent of the color change in standard samples after being exposed to artificial aging and make a comparison between standard samples before and after artificial aging. According to Italian guidelines, it should not exceed  $\Delta E$  on 5 [51].

### 2.10. Wettability measurements

The hydrophobic or hydrophilic properties of the stucco samples were tested before and after artificial aging by measuring the contact angle. This was done to see how well the surface would hold water using deionized water as a liquid probe and a compact video microscope (CVM 130 X). The samples were placed in the designated place, and then 3-microliter drops of water were placed on the surface of the samples using a graduated micropipette. Then a high-resolution image was taken, and finally the contact angles were calculated by the goniometer.

## 3. Results and Discussion

### 3.1. Preparation and characterization of BG/g-C<sub>3</sub>N<sub>4</sub> hybrid nanocomposites.

Fig. 3 a show the XRD patterns of virgin g-C<sub>3</sub>N<sub>4</sub>. Two peaks were found at approximately 13.1 and 27.4°, consistent with the crystalline structures of g-C<sub>3</sub>N<sub>4</sub> [52]. The high-intensity peak at 27.4°, which corresponded to an interlayer distance of 0.326 nm, reflected aromatic segment stacking and could be identified as the (002) peak observed in graphitic materials. The low-intensity peak at 13.1°, which corresponds to an interlayer spacing of 0.676 nm, was identified as the (100) peak and could be linked to an in-plane structural packing motif of tri-s-triazine units [42, 53]. In addition, FTIR spectroscopy was used to analyze the functional groups of the as-prepared g-C<sub>3</sub>N<sub>4</sub> samples, with the results shown in Fig. 3b. The typical spectra of each sample were comparable. Intense bands in the 1200-1700 cm<sup>-1</sup> area correspond to the stretching vibration modes of aromatic CN heterocycle repeating units [42, 54]. Triazine (C<sub>3</sub>N<sub>3</sub>) units typically exhibit a band around 800 cm<sup>-1</sup>, indicating their breathing mode. The peaks at 3100-3400 cm<sup>-1</sup> were due to a minor amount of residual amino (-NH<sub>2</sub>) group stretching vibration [42, 55].

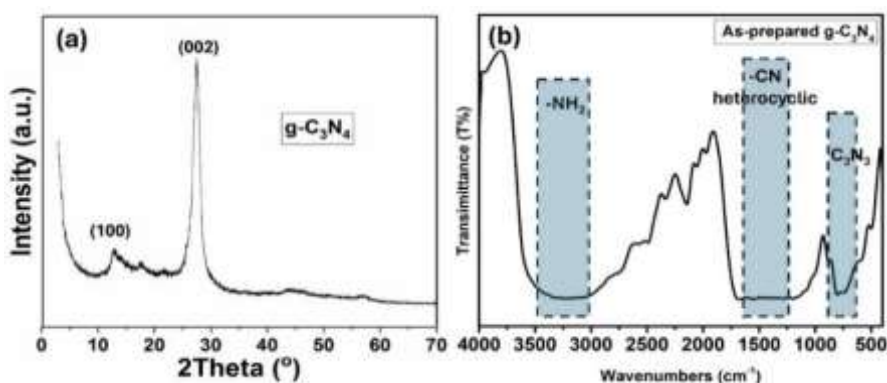


Fig. 3: XRD patterns (a) and FT-IR spectra (b) of as-prepared g-C<sub>3</sub>N<sub>4</sub> nanosheets

In addition, the colloidal properties such as hydrodynamic diameter ( $H_D$ ) and zeta potential ( $\eta$ ) data were determined using dynamic light scattering (DLS) technique. As shown in Fig. 4, the hydrodynamic diameter ( $H_D$ ) was about  $290 \pm 33.76$  nm, and the polydispersity index (PDI) about  $\sim 1.00$  (See Fig. 4a). Also, the zeta potential ( $\xi$ , mV) showed a moderate stability was about  $-14.8$  mV, as shown in Fig. 4b.

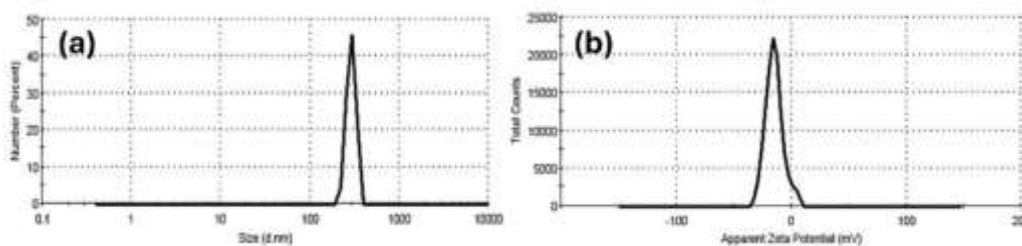


Fig. 4: DLS (a) and Zeta-potential (b) of as-prepared g-C<sub>3</sub>N<sub>4</sub> nanosheets

Furthermore, characterization of BG using X-ray diffraction indicated an amorphous structure, as illustrated in Fig. 5a. BG's FT-IR spectra reveal two distinct peaks (See Fig. 5b): one at 1038 cm<sup>-1</sup> for P-O stretching vibrations and another at 932 cm<sup>-1</sup> for Si-O-Si stretching of non-bridging oxygen atoms [40, 56, 57]. Other peaks at 742 and 500 cm<sup>-1</sup> are attributed to the Si-O-Si symmetric stretch of bridging oxygen atoms between tetrahedral and the P-O bending vibration, respectively [40, 58]. In addition, TEM image for as-prepared BG NPs is depicted in Fig. 5c. As clear from the figure, the predominant shapes for the as-prepared BG NPs vary between rod and spherical shapes, and the average particle size

was about 35.5 nm. Finally, the colloidal properties based on the particle size distributions and zeta potential for BG NPs are shown in Fig. 6. While the hydrodynamic diameter ( $H_D$ ) was about  $32.67 \pm 10$  nm with a polydispersity index (PDI) of 0.912. Also, BG NPs showed a low stability dispersion with a zeta potential of -6.39 mV.

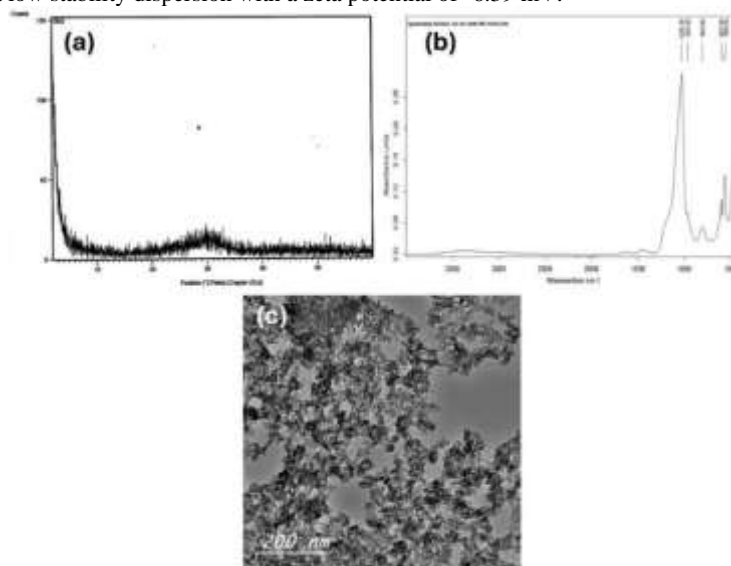


Fig. 5. XRD patterns (a) FT-IR spectra and (c) TEM images of as-prepared BG NPs

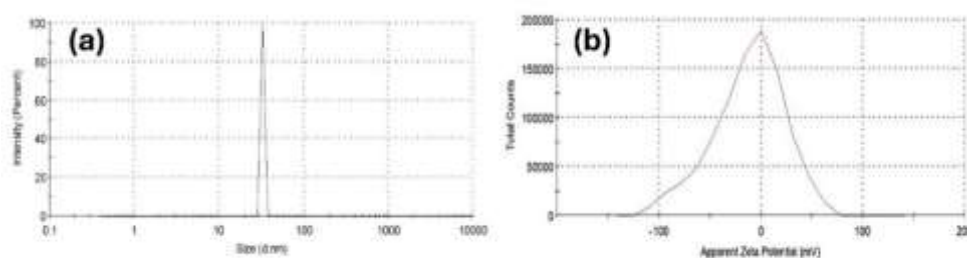


Fig. 6: DLS (a) and Zeta-potential (b) of as-prepared Bioactive glass NPs

### 3.2. USB digital microscope

- Discussion of the results of group (A) after applying the nanocomposite, after humidity-drying cycles, and after weathering cycles with sodium chloride salt, as shown in figure 7.

- Through virtual and visual examination with a digital camera and USB microscope, it was revealed after applying the nanocomposite that the pores and any air gaps were blocked, as well as the absence of cracks, pits, and cohesion in some of the fragmented parts, as shown in points (1, 2, 3). It became clear to us that in the experimental samples (A++), there was a thick layer on the surface with some minor cracks, and it appeared clearly through 500 X USB, as shown in point 4. After aging tests, a color change was observed, as shown in point 5. Surface cracks appear clearly, especially after the second test, as shown in point 6. Experimental samples (A+): Surface layer grains appear clearly, especially after the second test, as shown by points (7, 8).

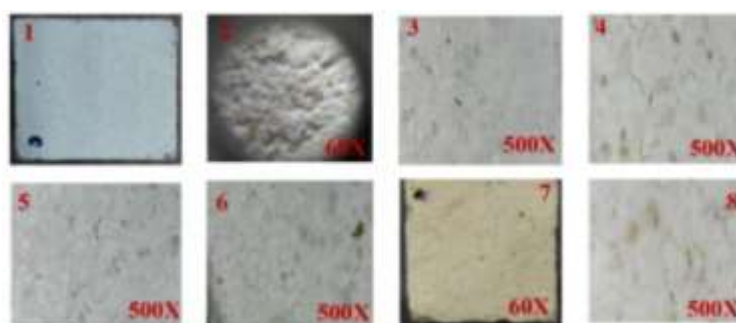


Fig. 7: shows the results of group (A) after applying the nanocomposite, after wet-drying cycles, and after weathering cycles with sodium chloride salt.

### Discussion of the results of group F after applying the nanocomposite, after humidity-drying cycles, and after weathering cycles with sodium chloride salt, as shown in figure 8.

Through virtual and visual examination with a digital camera and USB microscope, it was revealed after applying the nanocomposite that the pores and any air gaps were blocked, as well as the absence of cracks, pits, and cohesion in some of the fragmented parts, as shown in points (1, 2, 3). It became clear to us that a thick layer had formed on the surface, with some minor cracks, which appeared clearly through 500 x USB, as shown in point (4). After aging tests, a color change was observed, as shown in point 5.. When examining the experimental samples (F-F<sup>+</sup>), it became clear that a thick layer of nanocomposite was formed, full of cracks and separations, as shown in points (6, 7). As for the experimental samples (F<sup>++</sup>), it turns out that there is a thick layer of the compound, but it is cohesive and does not contain cracks or separations, as shown in point (8).



Fig. 8: shows the results of group (F) after applying the nanocomposite, after wet-drying cycles, and after weathering cycles with sodium chloride salt.

### 3.3. Evaluation of the efficacy of bioactive glass/g-C3N4 hybrid nanocomposites embedded in B72 matrix

Evaluation of the efficacy of bioactive glass/g-C3N4 hybrid nanocomposites embedded in B72 matrix has on the test samples, groups (A, F), The evaluation involved creating a 6-step protocol to assess the suitability of the reinforcement materials on experimental samples.

#### 3.3.1. Weight loss in the experimental sample group (A, F).

After comparing the average loss after placing the compound and after the artificial aging tests, as shown in Tables (2, 3), the average percentages varied slightly. - group (A<sup>+</sup>) had the most losses (1.29). group (A) had a loss percentage of 0.74. group (A<sup>++</sup>) had a loss percentage of 0.42; group (F) had the most loss (1.18); group (F<sup>+</sup>) had a percentage of (0.59); and the best group was (F<sup>++</sup>) by (0.41).

#### 3.3.2. Investigation of the surface morphology using a digital microscope and SEM

Examination using a USB digital microscope and SEM morphological examination of the experimental samples (groups A and F) before applying the nanocomposite and after artificial aging, as shown in Figures (9) and (10 points 1-2), and in comparison, between the experimental samples after applying the three concentrations of the nanocomposite and also after the artificial aging. By discussing the results of the visual examination or by SEM and identifying the general appearance, as shown in **Figures 9** and 10, the following becomes clear: **group (A):** When comparing the experimental samples before applying the nanocomposite, after applying the nanocomposite, and after artificial aging, it is concluded that the stability of the surface at the lowest concentration (0.5%: 1%: 3%), as shown in the experimental samples (A), and the concentration (1%: 1%: 3%), as shown in the experimental samples (A<sup>+</sup>), are both confirmed by the SEM examination. but when the percentage increased and became (3%: 1%: 3%) as shown in the experimental samples (A<sup>++</sup>), the compound was damaged and created a thick layer on the surface full of cracks and crevices. By also comparing the experimental samples before and after artificial aging, we also conclude that the experimental samples (A) after artificial aging still maintain their cohesion, but their cohesion has become clearer. We conclude from this that the added polymer has disappeared in the composite, and there are no cracks, breakages, or spaces between its atoms, which are not very simple. For the test samples (A<sup>+</sup>), their adhesion became clearer. This means that the added polymer in the composite went away, and small amounts of salts showed up on the surface. In the experimental samples (A<sup>++</sup>), the entire surface deteriorated and the percentages of salts on the surface increased. Concerning **group F**, it is concluded that SEM examination confirms the results through visual examination, which is the stability of the surface at the highest concentrations (3%, 2%, and 3%), as shown in the experimental samples (F<sup>++</sup>). It is clear to us through the morphological examination before aging that the polymer appears clearly in the samples (F). and (F<sup>+</sup>), in the case of samples after artificial aging, the added polymer disappears and the compound is present, but some salt atoms appear on the surface, and in the experimental samples (F<sup>++</sup>), the added polymer disappears after artificial aging, but the presence of layers of the compound is observed, as shown in the comparisons before and after artificial aging, so it was observed. The polymer disappears from the surface layer but is still present in the following layers, as shown in figure 10.

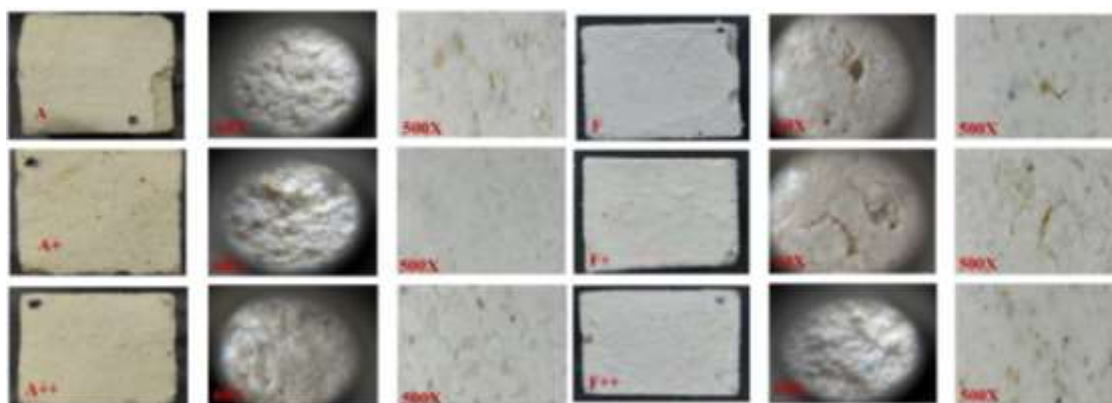


Fig. 9: shows the final evaluation of the nanocomposite after artificial aging through visual inspection, group (A, F).

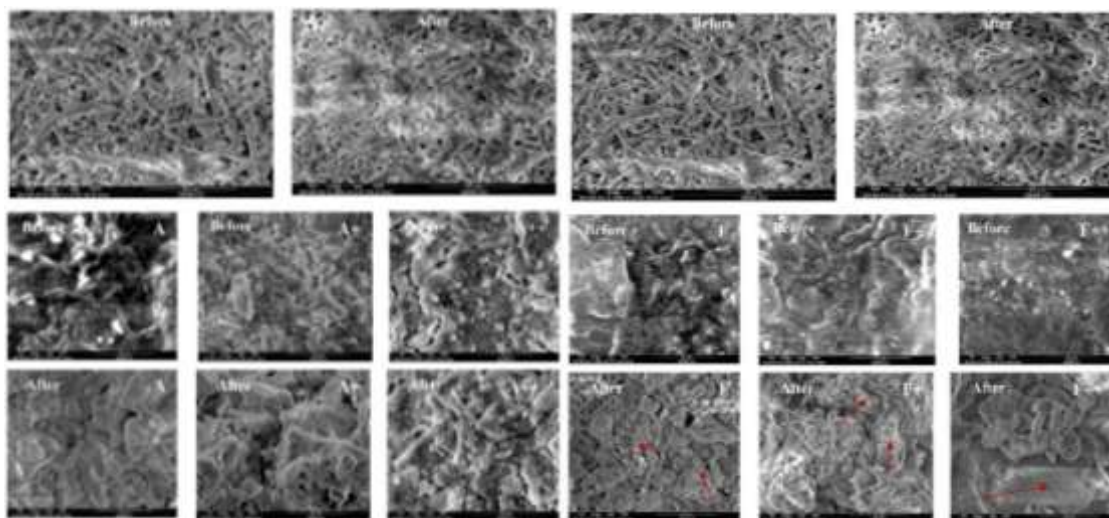


Fig. 10: group (A, F). shows a contrast between normal samples before and after Artificial aging (points 1-2), as well as between samples before and after using the nanocomposite and after Artificial aging them artificially using an SEM.

### 3.3.3. Change measurement.

As shown in Tables (4-5), change measurement group (A) revealed that when comparing the experimental samples after strengthening with nanocomposites and after accelerated artificial aging, we conclude that a colour change occurred in the experimental samples (A) with an average of (2.86), the experimental samples (A<sup>+</sup>) with an average of (2.69), and the experimental samples (A<sup>++</sup>) with an average of (1.98), We conclude from this that when the percentages of the compound increased, the percentages of colour change decreased, as shown in Table 4.

Table 4 shows the color change test for the experimental samples (group A) after strengthening with nanocomposites and after artificial aging.

$\Delta E$	After industrial aging			after strengthening with nanocomposites			group (A)
	L**	a**	b**	L*	a*	b*	
2.53	78.13	-29.51	3.59	80.93	-27.19	4.89	1A
2.83	80.09	-24.76	4.10	84.10	-26.31	5.14	2A
3.23	77.41	-30.65	3.74	81.47	-27.76	4.43	3A
1.90	79.38	-29.22	3.10	81.35	-32.50	3.91	1A <sup>+</sup>
1.64	80.04	-28.18	3.51	81.92	-30.43	3.71	2A <sup>+</sup>
4.54	78.15	-31.69	2.37	83.52	-27.83	4.56	3A <sup>+</sup>
1.02	81.15	-30.37	2.82	82.44	-31.09	3.84	1A <sup>++</sup>
1.95	80.78	-32.62	2.72	79.76	-29.12	3.44	2A <sup>++</sup>
2.98	80.22	-31.35	2.53	83.46	-28.50	4.26	3A <sup>++</sup>

**Change measurement group (F).** When comparing the experimental samples after strengthening with nanocomposites and after artificial aging, we conclude that a color change occurred in the experimental samples (F) with an average of (1.09), the experimental samples (F<sup>+</sup>) with an average of (2.88), and the experimental samples (F<sup>++</sup>) with an average of (3.27). We

conclude from this that when the percentages of the compound increased, the percentage of color change increased, as shown in Table 5.

Table 5 shows the color change test for the experimental samples (group F) after strengthening with nanocomposites and after artificial aging.

$\Delta E$	After industrial aging			after strengthening with nanocomposites			group (F)
	L**	a**	b**	L*	a*	b*	
1.50	81.43	-29.79	4.44	82.12	-27.58	5.44	1F
0.95	82.03	-28.50	4.91	81.85	-27.47	5.95	2F
0.82	79.33	-31.94	3.80	79.22	-30.03	3.60	3F
3.00	81.81	-27.56	5.05	79.96	-32.22	3.50	1F <sup>+</sup>
3.43	83.28	-26.56	4.79	80.01	-31.13	3.55	2F <sup>+</sup>
2.22	82.03	-27.18	4.39	84.92	-29.67	5.32	3F <sup>+</sup>
2.88	78.87	-33.50	2.03	82.42	-30.64	2.81	1F <sup>++</sup>
3.77	79.19	-33.99	1.94	83.32	-29.04	2.90	2F <sup>++</sup>
3.17	79.22	-32.67	2.29	83.29	-29.44	3.15	3F <sup>++</sup>

### 3-3-4 Determine the physical and mechanical properties of the experimental samples.

Determine the physical properties (water absorption and apparent porosity) and mechanical (compressive strength test) of the experimental samples after strengthening them with nanocomposite before and after artificial aging, group A-F. And compare them to the average results of standard samples without any additives that were subjected to aging. Industrial, as shown in graphs 11–12. After discussing the results of determining the physical and mechanical properties of the experimental samples before and after artificial aging, the compound bioactive glass/g-C3N4 hybrid nanocomposites embedded in the B72 matrix is a good compound with a concentration of 0.5%, 1%, and 3%. Group (A). This is because the average water absorption rate of the experimental samples is (23.10) and compared to the standard samples (30.23), and it has decreased by (7.13), and so on in their average porosity (29.12) and compared to the standard samples (36.70) and it decreased by (7.58) and we conclude from that that the percentage decreased and the experimental samples became in a better condition in terms of their physical properties, and also the average resistance of the samples to pressure (18.99) and compared to the standard samples (8.89) it increased by (10.10) and we conclude from that that the percentage increased and became The experimental samples are in better condition in terms of their mechanical properties. The average percentage of water absorption of the experimental samples after artificial aging (23.56) was compared to the samples before aging (23.10), and it increased by a very slight difference (0.46). Thus, in their average porosity (29.89) and compared to the samples before artificial aging (29.12), it increased by a very slight difference (0.77). We conclude from this that the experimental samples were not subjected to significant damage in terms of their physical properties, and the average resistance of the samples to pressure after artificial aging (10.55) compared to their samples before artificial aging (18.99) decreased by 8.44. We conclude from this that the experimental samples became weak in their mechanical properties but not in their condition before applying the compound to the samples, as the resistance of the standard samples to pressure before applying the compound and also after aging was 8.89 with a difference. Ratio (1.66). This confirms that the samples are in a better state of pressure resistance, knowing that the experimental samples on which the compound was applied were exposed to artificial aging twice, while before the compound they were exposed once, which confirms that the compound greatly improved their physical and mechanical properties

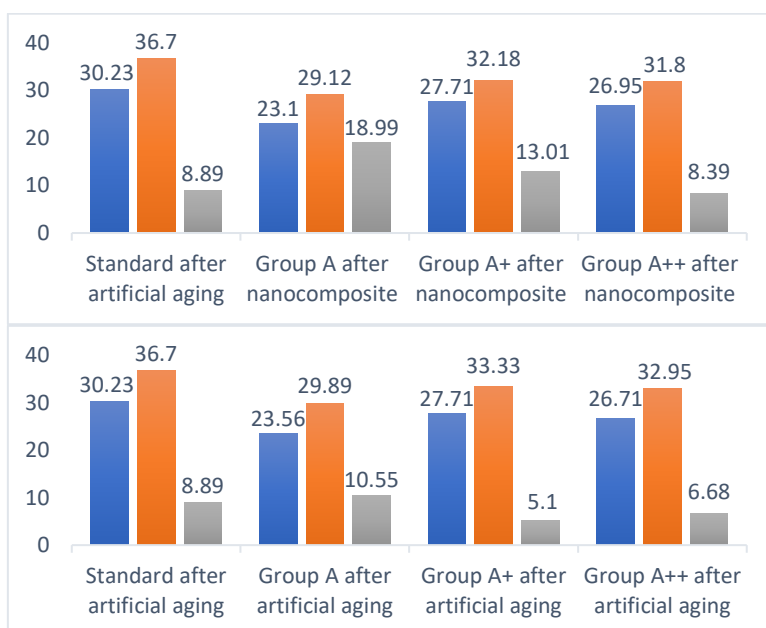


Fig. 11: shows physical properties (water absorption, and apparent porosity) and mechanical (compressive strength test) of the experimental samples. group A.

After discussing the results of determining the physical and mechanical properties of the experimental samples before and after artificial aging, compound bioactive glass/g-C3N4 hybrid nanocomposites embedded in B72 matrix compound with a concentration of 0.5%, 2%, and 3% was a good compound before artificial aging, but it deteriorated after artificial aging. As for the compound at a concentration of 1%, 2%, 3%, and 3%, it was a close compound for the experimental samples before putting the compound on them, as shown in the experimental samples (F<sup>+</sup>, F<sup>++</sup>).

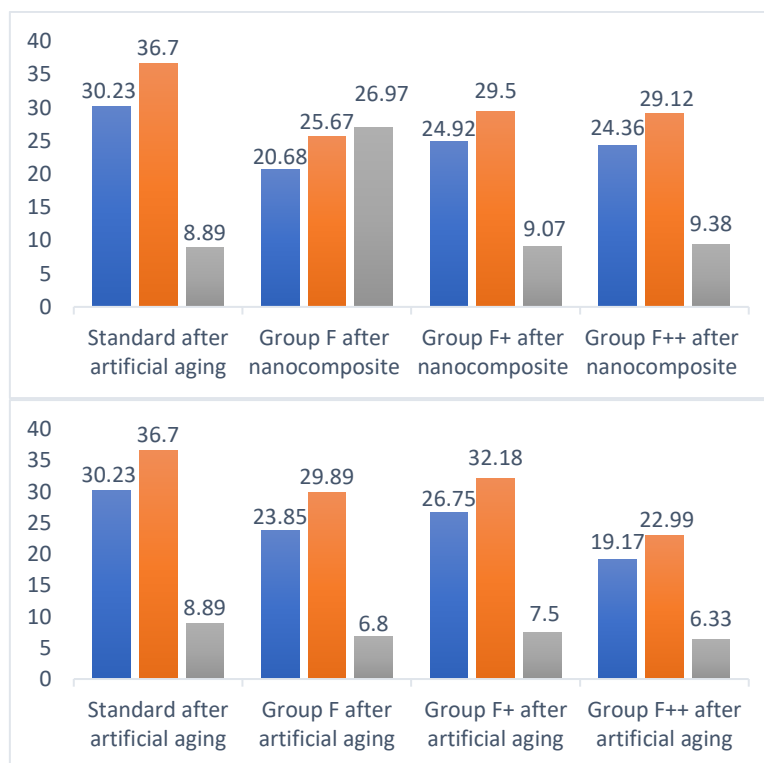


Fig. 12: shows physical properties (water absorption, and apparent porosity) and mechanical (compressive strength test) of the experimental samples group F.

### 3.3.5 Wettability measurements (Static water contact angle) group A-F.

#### Static water contact angle Group (A).

Water is one of the most harmful variables to stucco objects because it dissolves and recrystallizes various salts. It also promotes microbial activity. So, the consolidation materials used to preserve the stucco samples must have waterproof capabilities, keeping them protected from the impacts of water. When comparing the rate of hydrophobicity of the nanocomposite between the standard samples and the samples to which the nanocomposite was added, we notice a significant change, as shown in figure (13), where we notice the following:

1. There was a significant change in the measuring angles between the standard samples before artificial aging (60° -69°) and after artificial aging (51° -47°), with a difference of (9° -22°). This shows the extent of deterioration of the samples' surfaces and the rate of their hydrophobicity.

2: When comparing the angle measurements between standard samples after artificial aging (51° -47°), group (A) (105° -114°) with a difference of (54° -67°), group (A<sup>+</sup>) (99° -103°) with a difference of (48° -56°), and group (A<sup>++</sup>), (74° -74°) with a difference of (23° -27°). It is clear to us that there is an increase in the rate of hydrophobicity of the samples after applying the compound and before performing the artificial aging work. We conclude that the best is group (A) by a very large difference, followed by group (A<sup>+</sup>), then after that group (A<sup>++</sup>).

3. When comparing the angle measurements between the experimental samples before and after aging, it becomes clear to us that group (A) had a change in angles with a difference of (2° -12°), group (A<sup>+</sup>) with a difference of (19° -19°), and group (A<sup>++</sup>) with a difference of (2° -4°).

We conclude that the best is group (A), which is the group with no change in its hydrophobicity rate before and after artificial aging, and also the angle or hydrophobicity rate is high.

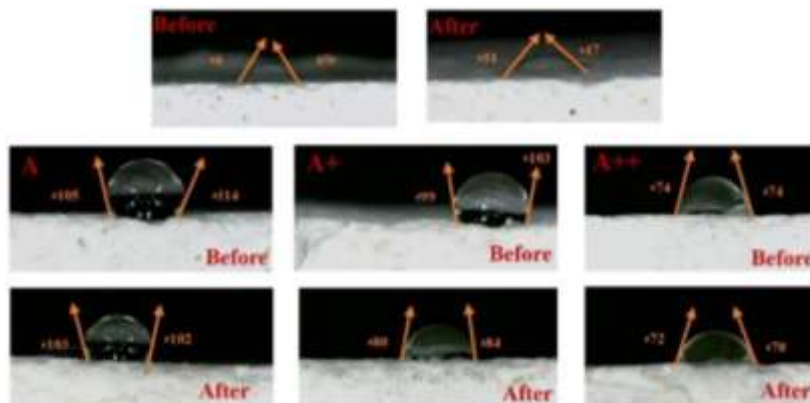


Fig. 13: shows the average hydrophobicity of the prepared nanocomposites. Group A.

**Static water contact angle Group (F).** When comparing the rate of hydrophobicity of the nanocomposite between the standard samples and the samples to which the nanocomposite was added, we notice a significant change, as shown in figure (14), where we notice the following:

1. There was a significant change in the measuring angles between the standard samples before artificial aging ( $60^\circ$  - $69^\circ$ ) and after artificial aging ( $51^\circ$  - $47^\circ$ ), with a difference of ( $9^\circ$  - $22^\circ$ ). This shows the extent of deterioration of the samples' surfaces and the rate of their hydrophobicity.

2: When comparing the angle measurements between standard samples after aging ( $51^\circ$  - $47^\circ$ ), group (F) ( $101^\circ$  - $100^\circ$ ) with a difference of ( $50^\circ$  - $53^\circ$ ), group (F+) ( $92^\circ$  - $93^\circ$ ) with a difference of ( $41^\circ$  - $46^\circ$ ), and group (F++) ( $90^\circ$  - $99^\circ$ ) with a difference of ( $39^\circ$  - $52^\circ$ ). It is clear to us that there is an increase in the rate of hydrophobicity of the samples after applying the compound and before performing the artificial aging work. We conclude that the best is group (F), followed by group (F++), and after that group (F+).

3. When comparing the angle measurements between the experimental samples before and after artificial aging, it becomes clear to us that group (F) had a change in angles with a difference of ( $20^\circ$  - $23^\circ$ ), group (F+) with a difference of ( $22^\circ$  - $20^\circ$ ), and group (F++) with a difference of ( $2^\circ$  - $13^\circ$ ). We conclude that the best is the group (F++), which is the group with no change in its hydrophobicity rate before and after artificial aging and also whose angle or hydrophobicity rate is high.

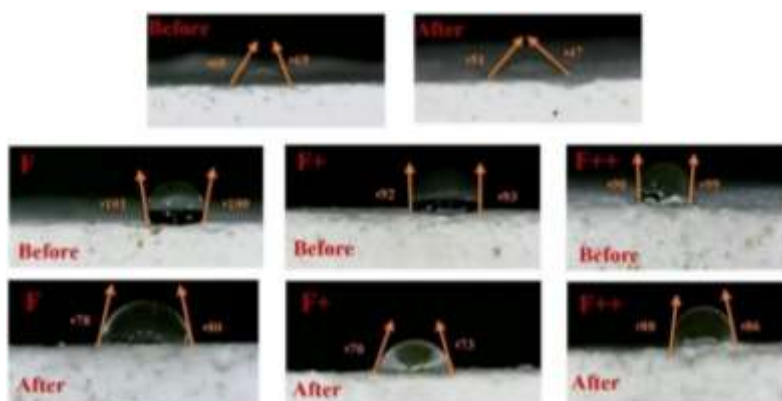


Fig. 14: shows the average hydrophobicity of the prepared nanocomposites. Group F

#### 4. Conclusion

Water and salt crystallization were among the many forms of deterioration to archaeological stucco. These harmful variables have an impact on the endurance and strength of stucco, resulting in products that are fragile and weak. Therefore, it was important to utilize consolidation materials to safeguard these stucco objects. The final conclusion comes from evaluating the effectiveness and effect of bioactive glass/g-C3N4 hybrid nanocomposites embedded in B72 on experimental samples. It became clear to us through the 6-step protocol that the compound (BG NPs) 0.5% + (g-C3N4) 1% + B 72, 3% is the best in consolidating in terms of measuring the weight of experimental samples, where the percentage of weight loss was (0.74), general appearance, and morphological examination by electron microscope. In the scanner, the composite was distinguished by its efficiency, depth of penetration, ability of the material to spread, and extent of bonding between the material and the treated surface in terms of determining the physical and mechanical properties, as well as in terms of the rate of hydrophobicity of the nanocomposite (contact angle), but with a simple color change rate of up to 2.86. So, the results showed that nano-composites enhanced the hydrophobic character as colorimetric measurement appears that (BG NPs) 0.5% + (g-C3N4) 1% + B 72, 3% that means that this group acceptable as a consolidate material to consolidate archaeological stucco.

#### Author Contribution

##### Conflicts of interest

There are no conflicts to declare.

#### Funding

No Fund

#### Acknowledgments

We would like to express our heartfelt appreciation to the anonymous reviewers, whose suggestions significantly improved this work.

#### References

- [1] R.-M. Ion, T. Nyokong, N. Nwahara, I.-R. Suica-Bunghez, L. Iancu, S. Teodorescu, I.D. Dulama, R.M. Stirbescu, A. Gheboianu, R.M. Grigorescu, Wood preservation with gold hydroxyapatite system, *Heritage Science* 6(1) (2018) 1-12.
- [2] M.E. David, R.-M. Ion, R.M. Grigorescu, L. Iancu, E.R. Andrei, Nanomaterials used in conservation and restoration of cultural heritage: An up-to-date overview, *Materials* 13(9) (2020) 2064.
- [3] K. Kroftová, T. Čejka, Materials and technologies for the consolidation of historic plasters by the wetting and surface penetration method, *Stavební obzor-Civil Engineering Journal* 29(4) (2020).
- [4] H.H.M. Mahmoud, A.M. Kamel, M.F. Ali, Developing Low-Cost Eco-friendly Restoration Mortars for Historic Lime-based Stucco and Building Materials, *Periodica Polytechnica Civil Engineering* (2024).
- [5] H. England, *Practical Building Conservation: Mortars, Plasters and Renders*, Ashgate Publishing, Ltd.2012.
- [6] V. Gírsa, D. Michoinová, *Historické omítky: záchrana, konzervace, obnova:(metodika přístupu k historickým omítkám ak jejich záchraně)*, České vysoké učení technické v Praze 2013.
- [7] J. Mathew, J. Joy, S.C. George, Potential applications of nanotechnology in transportation: A review, *Journal of King Saud University-Science* 31(4) (2019) 586-594.
- [8] P. Baglioni, D. Chelazzi, R. Giorgi, *Nanotechnologies in the Conservation of Cultural Heritage: A compendium of materials and techniques*, Springer 2015.
- [9] S. Rajendran, T.A. Nguyen, S. Kakooci, M. Yeganeh, Y. Li, *Corrosion protection at the nanoscale*, Elsevier2020.
- [10] R.-M. Ion, S.-M. Doncea, D. Țurcanu-Caruțiu, *Nanotechnologies in cultural heritage-Materials and instruments for diagnosis and treatment, Novel Nanomaterials*; IntechOpen: London, UK (2018) 173-190.
- [11] A. Blee, J. Matisons, Nanoparticles and the conservation of cultural heritage, *Materials forum*, 2008, pp. 121-128.
- [12] M. Reyes-Estebanez, B.O. Ortega-Morales, M. Chan-Bacab, C. Granados-Echegoyen, J.C. Camacho-Chab, J.E. Pereañez-Sacarias, C. Gaylarde, Antimicrobial engineered nanoparticles in the built cultural heritage context and their ecotoxicological impact on animals and plants: A brief review, *Heritage Science* 6 (2018) 1-11.
- [13] S. Leydecker, *Nano materials: in architecture, interior architecture and design*, Springer Science & Business Media2008.
- [14] M. Reibold, P. Paufler, A.A. Levin, W. Kochmann, N. Pätzke, D. Meyer, Carbon nanotubes in an ancient Damascus sabre, *Nature* 444(7117) (2006) 286-286.
- [15] V. Dos Santos, R.N. Brandalise, M. Savaris, *Engineering of biomaterials*, Springer2017.
- [16] J.R. Jones, Review of bioactive glass: from Hench to hybrids, *Acta biomaterialia* 9(1) (2013) 4457-4486.
- [17] E.A. Abou Neel, D.M. Pickup, S.P. Valappil, R.J. Newport, J.C. Knowles, Bioactive functional materials: a perspective on phosphate-based glasses, *Journal of Materials Chemistry* 19(6) (2009) 690-701.
- [18] I. Xynos, M. Hukkanen, J. Batten, L. Buttery, L. Hench, J. Polak, Bioglass® 45S5 stimulates osteoblast turnover and enhances bone formation in vitro: implications and applications for bone tissue engineering, *Calcified tissue international* 67 (2000) 321-329.
- [19] A. Hoppe, A.R. Boccaccini, Biological impact of bioactive glasses and their dissolution products, *Biomaterials for Oral and Craniomaxillofacial Applications* 17 (2015) 22-32.
- [20] D. Bellucci, A. Sola, V. Cannillo, Hydroxyapatite and tricalcium phosphate composites with bioactive glass as second phase: State of the art and current applications, *Journal of Biomedical Materials Research Part A* 104(4) (2016) 1030-1056.

- [21] M.H. Kaou, M. Furkó, K. Balázs, C. Balázs, *Advanced Bioactive Glasses: The Newest Achievements and Breakthroughs in the Area*, *Nanomaterials* (Basel) 13(16) (2023).
- [22] M.T. Islam, R.M. Felfel, E.A. Abou Neel, D.M. Grant, I. Ahmed, K.M.Z. Hossain, *Bioactive calcium phosphate-based glasses and ceramics and their biomedical applications: A review*, *J Tissue Eng* 8 (2017) 2041731417719170.
- [23] R.-M. Ion, S.M. Doncea, M.-L. Ion, V. Rădițoiu, V. Amăriuței, *Surface investigations of old book paper treated with hydroxyapatite nanoparticles*, *Applied Surface Science* 285 (2013) 27-32.
- [24] A. North, M. Balonis, I. Kakoulli, *Biomimetic hydroxyapatite as a new consolidating agent for archaeological bone*, *Studies in Conservation* 61(3) (2016) 146-161.
- [25] Y. Ezhumalai, P. Kumaresan, T. Jayapalan, *Graphite Carbon Nitride, Photocatalysts-New Perspectives*, IntechOpen2022.
- [26] S.-M. Lam, J.-C. Sin, A.R. Mohamed, *A review on photocatalytic application of g-C<sub>3</sub>N<sub>4</sub>/semiconductor (CNS) nanocomposites towards the erasure of dyeing wastewater*, *Materials Science in Semiconductor Processing* 47 (2016) 62-84.
- [27] J. He, *Preparation and photocatalysis of graphite carbon nitride based photocatalysts*, Curtin University, 2015.
- [28] N. Talreja, D. Chauhan, M. Ashfaq, *Photo-Antibacterial Activity of Two-Dimensional (2D)-Based Hybrid Materials: Effective Treatment Strategy for Controlling Bacterial Infection*, *Antibiotics* (Basel) 12(2) (2023).
- [29] S.P. Koob, *The use of Paraloid B-72 as an adhesive: its application for archaeological ceramics and other materials*, *Studies in conservation* 31(1) (1986) 7-14.
- [30] M. LAURENZI TABASSO, U. Santamaria, *Consolidant and protective effects of different products on Lecce limestone*, *Congrès international sur l'altération et la conservation de la pierre*. 5, 1985, pp. 697-707.
- [31] E. Lombardi, *BIOTECHNOLOGIES FOR RESTORATION OF CULTURAL HERITAGE*, (2014).
- [32] T. Hanemann, D.V. Szabó, *Polymer-nanoparticle composites: from synthesis to modern applications*, *Materials* 3(6) (2010) 3468-3517.
- [33] R. Singh, S.G. Kulkarni, S.S. Channe, *Thermal and mechanical properties of nano-titanium dioxide-doped polyvinyl alcohol*, *Polymer bulletin* 70 (2013) 1251-1264.
- [34] N. Azadi, H. Parsimehr, A. Ershad-Langroudi, *Cultural heritage protection via hybrid nanocomposite coating*, *Plastics, Rubber and Composites* 49(9) (2020) 414-424.
- [35] J.Z. Guo, K. Song, C. Liu, *Polymer-based multifunctional nanocomposites and their applications*, Elsevier2018.
- [36] S.A.B. Hasan, M.M. Dimitrijević, A. Kojović, D.B. Stojanović, K. Obradović-Đuričić, R.M.J. Heinemann, R. Aleksić, *The effect of the size and shape of alumina nanofillers on the mechanical behavior of PMMA matrix composites*, *Journal of the Serbian Chemical Society* 79(10) (2014) 1295.
- [37] A. Mathiazhagan, R. Joseph, *Nanotechnology-a New prospective in organic coating-review*, *International Journal of Chemical Engineering and Applications* 2(4) (2011) 225.
- [38] A.M. El-Kady, A.F. Ali, M.M. Farag, *Development, characterization, and in vitro bioactivity studies of sol-gel bioactive glass/poly (L-lactide) nanocomposite scaffolds*, *Materials Science and Engineering: C* 30(1) (2010) 120-131.
- [39] M. Mabrouk, A. Mostafa, H. Oudadesse, E. Wers, A. Lucas-Girot, M.I. El-Gohary, *Comparative study of nanobioactive glass quaternary system 46S6*, *Bioceramics Development and Applications* 4(1) (2014) 1000072.
- [40] M.M. El-Sayed, A.A. Mostafa, A.M. Gaafar, W. El Hotaby, E.M. Hamzawy, M.S. El-Okaily, A.M. Gamal-Eldeen, *in vitro kinetic investigations on the bioactivity and cytocompatibility of bioactive glasses prepared via melting and sol-gel techniques for bone regeneration applications*, *Biomedical Materials* 12(1) (2017) 015029.
- [41] A.M. El-Kady, M.M. Farag, *Bioactive glass nanoparticles as a new delivery system for sustained 5-fluorouracil release: characterization and evaluation of drug release mechanism*, *Journal of Nanomaterials* 16(1) (2016) 399-399.
- [42] Z. Wang, Y. Huo, Y. Fan, R. Wu, H. Wu, F. Wang, X. Xu, *Facile synthesis of carbon-rich g-C<sub>3</sub>N<sub>4</sub> by copolymerization of urea and tetracyanoethylene for photocatalytic degradation of Orange II*, *Journal of Photochemistry and Photobiology A: Chemistry* 358 (2018) 61-69.
- [43] T. Wang, B. Song, L. Wang, *A new filler for epoxy resin: Study on the properties of graphite carbon nitride (g-c<sub>3</sub>n<sub>4</sub>) reinforced epoxy resin composites*, *Polymers* 12(1) (2020) 76.
- [44] M.S. Ali Khedr, M.F. Aly, A.M. Kamel, M. Elghanam, *Characterization Study of a Roman Stucco Death Mask from the National Museum of Egyptian Civilization*, *Egyptian Journal of Chemistry* (2024).
- [45] V. Fassina, *Stone material in monuments: Diagnosis and conservation*, *Scuola universitaria CUM conservazione dei monumenti*. Heraklion, Crete (1993) 24-30.
- [46] M.A. De Buergo, R. Fort, M. Gómez-Heras, *Contributions of scanning electron microscopy to the assessment of the effectiveness of stone conservation treatments*, *Scanning: The Journal of Scanning Microscopies* 26(1) (2004) 41-47.
- [47] M. Lettieri, M. Masieri, *Performances and coating morphology of a siloxane-based hydrophobic product applied in different concentrations on a highly porous stone*, *Coatings* 6(4) (2016) 60.
- [48] M.M. Ibrahim, W.S. Mohamed, H.M. Mohamed, *Evaluation of the Efficacy of Traditional and Nano Paraloid B72 for Pottery Consolidation*, *International Journal of Conservation Science*, Vol. 13, (2022), 15-30.
- [49] S. Hemed, M. Khalil, A. Shoeb, A. Abd El Aziz, *The Effectiveness of Nano Materials and Nano-Modified Polymers for Preservation of Historical Brick Masonry in Rashid, Egypt*, *International Journal of Conservation Science*, Vol. 9, No. 4, (2018), 835-846.
- [50] W. D. Kessler, A. Hackman, E. R. Anderson, *Building Materials and Structures*, United States Department of Commerce, Secretary National Bureau of Standards, United States Government Printing Office, Washington, (1943) 7.
- [51] N. Misura, *colormetric he strumentali di superfici opache*, Available online 2017: [http://www.architettiroma.it/fpdb/consultabc/File/ConsultaBC/Lessico\\_NorMal-Santopuoli.pdf](http://www.architettiroma.it/fpdb/consultabc/File/ConsultaBC/Lessico_NorMal-Santopuoli.pdf).

- [52] X. Wang, X. Chen, A. Thomas, X. Fu, M. Antonietti, Metal-containing carbon nitride compounds: a new functional organic-metal hybrid material, *Advanced Materials* 21(16) (2009) 1609-1612.
- [53] Q. Xiang, J. Yu, M. Jaroniec, Preparation and enhanced visible-light photocatalytic H<sub>2</sub>-production activity of graphene/C<sub>3</sub>N<sub>4</sub> composites, *The Journal of Physical Chemistry C* 115(15) (2011) 7355-7363.
- [54] M.J. Bojdys, J.O. Müller, M. Antonietti, A. Thomas, Ionothermal synthesis of crystalline, condensed, graphitic carbon nitride, *Chemistry—A European Journal* 14(27) (2008) 8177-8182.
- [55] Y. Zheng, Z. Zhang, C. Li, S. Proulx, Surface hydroxylation of graphitic carbon nitride: Enhanced visible light photocatalytic activity, *Materials Research Bulletin* 84 (2016) 46-56.
- [56] L. Radev, V. Hristov, I. Michailova, H.M.V. Fernandes, M.I.M. Salvado, In vitro bioactivity of biphasic calcium phosphate silicate glass-ceramic in CaO-SiO<sub>2</sub>-P<sub>2</sub>O<sub>5</sub> system, *Processing and Application of Ceramics* 4(1) (2010) 15-24.
- [57] M. Mami, H. Oudadesse, R. Dorbez-Sridi, H. Capioux, P. Pellen-Mussi, D. Chauvel-Lebret, H. Chaair, G. Cathelineau, Synthesis and in-vitro characterization of melt derived 47S CaO-P<sub>2</sub>O<sub>5</sub>-SiO<sub>2</sub>-Na<sub>2</sub>O bioactive glass, *Ceram-Silik* 52(3) (2008) 121-9.
- [58] J. Ding, Y. Chen, W. Chen, L. Hu, G. Boulon, Effect of P<sub>2</sub>O<sub>5</sub> addition on the structural and spectroscopic properties of sodium aluminosilicate glass, *Chinese Optics Letters* 10(7) (2012) 071602-071602.